Highly efficient vortex four-wave mixing in asymmetric semiconductor quantum wells

JING QIU,[1] ZHIPING WANG,[1,2,*] DONGSHENG DING,[3] WEIBIN LI,[2]
AND BENLI YU[1]

[1]*Key Laboratory of Opto-Electronic Information Acquisition and Manipulation of Ministry of Education, Anhui University, Hefei 230601, China*
[2]*School of Physics and Astronomy, University of Nottingham, Nottingham NG7 2RD, UK*
[3]*Key Laboratory of Quantum Information, University of Science and Technology of China, Hefei, Anhui 230026, China*
[*]wzping@mail.ustc.edu.cn

Abstract: Orbital angular momentum (OAM) is an important property of vortex light, which provides a valuable tool to manipulate the light-matter interaction in the study of classical and quantum optics. Here we propose a scheme to generate vortex light fields via four-wave mixing (FWM) in asymmetric semiconductor quantum wells. By tailoring the probe-field and control-field detunings, we can effectively manipulate the helical phase and intensity of the FWM field. Particularly, when probe field and control field have identical detuning, we find that both the absorption and phase twist of the generated FWM field are significantly suppressed. Consequently, the highly efficient vortex FWM is realized, where the maximum conversion efficiency reaches around 50%. Our study provides a tool to transfer vortex wavefronts from input to output fields in an efficient way, which may find potential applications in solid-state quantum optics and quantum information processing.

1. Introduction

Vortex beams carrying orbital angular momentum (OAM) [1,2] are now widely explored for different domains [3–7]. Unlike the conventional beam, the OAM beam provides a larger orthonormal spatial basis. Recently rapid progresses have been made to explore interactions between atomic gases and laser light with OAM. For example, the storage and memory based on OAM have been demonstrated in atomic vapors [8–10]. The transfer of OAM has been studied in multilevel atomic systems [11,12] . Research into the spatially structured transparency in a cold rubidium atomic system has been introduced [13]. Moreover, vortex four-wave mixing (FWM) has been investigated in [85]Rb vapor, they found that the phase profile associated with OAM is transferred entirely from the one light to another [14]. Quite recently, the vortex six-wave mixing (SWM) and its manipulation in an atomic system has also been experimentally observed [15].

On the other hand, there have been a lot of efforts on quantum coherent phenomena in semiconductor quantum wells (SQWs). The important motivations of using SQWs are that their transition energies, dipole moments, and symmetries can be engineered as desired and the dipole moments of intersubband transitions are large. Quantum coherent phenomena (e.g., lasing without inversion [16–18], coherent population trapping [20], enhancement of refractive index [19], electromagnetically induced transparency [21,22], and slow light [23], etc.) in semiconductor heterostructures have been explored both theoretically and experimentally. Benefiting from the inherent advantages of the SQWs, it has been suggested that enhanced Kerr nonlinearity [24,25], optical bistability [26], and slow optical solitons [27,28] are possible in such systems. In addition, a number of studies have also analyzed FWM in a variety of SQWs [29–32]. However, the spatial characteristics of the FWM field have not been fully studied during the FWM process in solid-state systems. Inspired by this, here we put forward a new scheme to achieve the

high-efficiency vortex FWM generation in SQWs. In comparison with most scenarios in atomic gases [33–38] , the major advantages of our scheme are as follows. (i) The basic structure of the SQW is a double-well potential, where strong cross coupling between the neighboring wells are present [see Fig. 1(a)]. The cross coupling arises from two transitions between one ground state and two energetically closed excited states, which can create a strong coherence between the two closely spaced excited states. (ii) By coupling these states with the laser lights, we show that a new light field can be efficiently generated through mixing the input laser light. Through tuning the probe-field and control-field detunings, we can effectively manipulate the generated FWM field and the maximum conversion efficiency is approximately 50%. (iii) The SQWs are preferred for practical applications due to the flexible manufactuation and controllable interference strength [39]. As a result, our scheme may open up a new perspective for modulating the vortex FWM in a solid device.
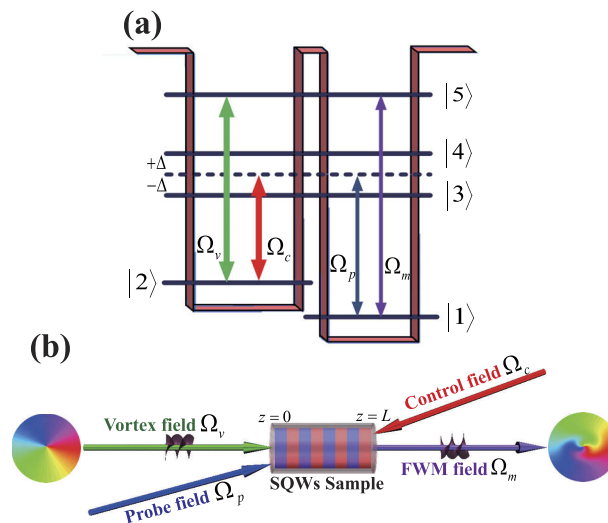
Fig. 1. (a) The fundamental structure is coupled asymmetric quantum wells. Each well has a distinctive ground state, labeled as $|1\rangle$ and $|2\rangle$. The first excited state of the well is nearly degenerate. The cross coupling between the well leads to delocalized state $|3\rangle$ and $|4\rangle$. Another state $|5\rangle$ is used to produce the FWM field. A probe field Ω_p connects states $|1\rangle$ and $|3\rangle$, while a control field Ω_c couples states $|2\rangle$ and $|3\rangle$. A vortex field Ω_v drives states $|2\rangle$ and $|5\rangle$, and the FWM field is generated from the transition $|5\rangle \leftrightarrow |1\rangle$. (b) Geometry of the laser fields. The FWM field carrying OAM is generated under the phase-matching condition $\vec{k}_p + \vec{k}_v = \vec{k}_c + \vec{k}_m$.

The structure of the article is organized as follows. In Section II, we describe the system and corresponding model. The dynamics of the system are governed by the coupled Schrödinger equations. In the slowly varying amplitude approximation, we derive the light propagation equation based on the Maxwell equation. Results are shown in Section III. We analyze spatial properties of the FWM output field, focusing on helical phase and spatial intensity distributions. We discuss how the different parameters affect the spatial-dependent absorption and phase properties of the FWM field. It's found that high conversion efficiency can be achieved by tuning systemic parameters. Finally we conclude in Section IV.

2.   Model and dynamic equations

We consider an asymmetric semiconductor quantum well as shown in Fig. 1, which consists of a shallow well (a 11.0 nm $Al_{0.04}Ga_{0.96}As$ layer) and a deep well (a 9.5 nm GaAs layer), and they are separated by a 3.8 nm $Al_{0.4}Ga_{0.6}As$ potential barrier [40]. Both the shallow well (left) and the deep well (right) are $Al_{0.4}Ga_{0.6}As$ potential barriers. Due to the tunneling effect, the SQW structure has five subbands which include two ground subbands $|1\rangle$ and $|2\rangle$, two closely separated excited subbands $|3\rangle$ and $|4\rangle$, and a second excited subband $|5\rangle$. By solving the effective mass Schrö dinger equations [41], we can obtain that the energies of five subbands are $E_1 = 34.5$ meV, $E_2 = 62.3$ meV, $E_3 = 135.5$ meV, $E_4 = 141.5$ meV and $E_5 = 296.3$ meV, respectively. We study the coupling of these states with external laser lights. Subbands $|3\rangle$ and $|4\rangle$ are separated by an energy splitting 2Δ, which are coupled with two ground subbands $|1\rangle$ and $|2\rangle$ by a weak super-Gaussian pulse field with Rabi frequency $\Omega_p = \Omega_0 \exp[-(x^2 + y^2)^8/\omega_{sp}^{16}]e^{-t^2/\tau^2}$ (ω_{sp} and Ω_0 are the transverse waist and initial amplitude of the field, and τ is pulse length) and a continuous-wave control field with Rabi frequency Ω_c, respectively. The transition $|2\rangle \leftrightarrow |5\rangle$ is driven by a vortex field Ω_v. Then a FWM field Ω_m can be efficiently generated via the nonlinear process. Here, the vortex field is a Laguerre-Gaussian (LG) mode and its Rabi frequency is [42]

$$\Omega_v = \sqrt{2p!/\pi(p+|l|)!}\frac{\Omega_{v0}}{\omega_0}\left(\frac{\sqrt{2}r}{\omega_0}\right)^{|l|}\exp\left(-\frac{r^2}{\omega_0^2}\right)L_p^{|l|}\left(\frac{2r^2}{\omega_0^2}\right)\exp(-il\phi), \quad (1)$$

where Ω_{v0} is the initial amplitude, r is the radial radius and the beam waist is given by ω_0. ϕ is the azimuthal angle and $L_p^{|l|}$ is a generalized Laguerre polynomial. The radial index and azimuthal index are defined by p and l, respectively.

In the present analysis we assume that the SQWs with low dopings are designed such that electron-electron effects have very small influences on our results. Many-body effects for example, the depolarization effect, which renormalizes the free-carrier and carrier-field contributions are not included in our study [43]. Under the rotating wave and electric-dipole approximations, the Hamiltonian in the interaction picture can be written as ($\hbar = 1$)

$$
\begin{aligned}
H_I = {} & (\Delta_p - \Delta_c)|2\rangle\langle2| + (\Delta_p - \Delta)|3\rangle\langle3| + (\Delta_p + \Delta)|4\rangle\langle4| \\
& + (\Delta_v + \Delta_p - \Delta_c)|5\rangle\langle5| - (g\Omega_p e^{i\vec{k}_p\cdot\mathbf{r}}|3\rangle\langle1| \\
& + \Omega_p e^{i\vec{k}_p\cdot\mathbf{r}}|4\rangle\langle1| + f\Omega_c e^{i\vec{k}_c\cdot\mathbf{r}}|3\rangle\langle2| + \Omega_c e^{i\vec{k}_c\cdot\mathbf{r}}|4\rangle\langle2| \\
& + \Omega_v e^{i\vec{k}_v\cdot\mathbf{r}}|5\rangle\langle2| + \Omega_m e^{i\vec{k}_m\cdot\mathbf{r}}|5\rangle\langle1| + H.c.),
\end{aligned}
\quad (2)
$$

where the detunings of relevant fields are denoted as $\Delta_p = [(E_3 + E_4)/2 - E_1] - \omega_p$, $\Delta_c = [(E_3 + E_4)/2 - E_2] - \omega_c$ and $\Delta_v = E_5 - E_2 - \omega_v$. $E_j(j = 1 - 5)$ is the energy of subband $|j\rangle$. The ratios of the transition dipole moments between the relevant subbands are defined as $g = \mu_{13}/\mu_{41}$ and $f = \mu_{32}/\mu_{42}$, in which $\mu_{nb}(n, b = 1 - 5, n \neq b)$ represents the dipole moment for the transition between states $|n\rangle \leftrightarrow |b\rangle$. The wave vectors of the corresponding fields are $\vec{k}_j(j = p, c, v, m)$.

Defining the electronic energy state as $|\psi\rangle = A_1|1\rangle + A_2 e^{i(\vec{k}_p-\vec{k}_c)\cdot\mathbf{r}}|2\rangle + A_3 e^{i\vec{k}_p\cdot\mathbf{r}}|3\rangle + A_4 e^{\vec{k}_p\cdot\mathbf{r}}|4\rangle + A_5 e^{i(\vec{k}_p-\vec{k}_c+\vec{k}_v)\cdot\mathbf{r}}|5\rangle$ and using the Schrödinger equation $i\hbar\partial|\psi\rangle/\partial t = H_I|\psi\rangle$, the equations of motion for the probability amplitude A_j ($j = 1 - 5$) can be obtained as [44]

$$\dot{A}_2 = -i(\Delta_p - \Delta_c)A_2 + if\Omega_c^*A_3 + i\Omega_c^*A_4 + i\Omega_v^*A_5 - \gamma_2 A_2, \quad (3)$$

$$\dot{A}_3 = -i(\Delta_p - \Delta - i\gamma_3)A_3 + ig\Omega_p A_1 + if\Omega_c A_2, \quad (4)$$

$$\dot{A}_4 = -i(\Delta_p + \Delta - i\gamma_4)A_4 + i\Omega_p A_1 + i\Omega_c A_2, \quad (5)$$

$$\dot{A}_5 = -i(\Delta_v + \Delta_p - \Delta_c)A_5 + i\Omega_v A_2 + i\Omega_m A_1 - \gamma_5 A_5, \tag{6}$$

The effective decay rate γ_j ($j = 2 - 5$) for each subband $|j\rangle$ are phenomenologically added to the above equations [45–47], which comprise of a population-decay contribution γ_{jl} and a dephasing contribution γ_{jd}, i.e. $\gamma_j = \gamma_{jl} + \gamma_{jd}$. γ_{jl} tends to only occur at low temperatures due to longitudinal optical photon emissions, while γ_{jd} is attributed to a combination of quasi-elastic interface roughness scattering and electron-photon scattering.

Using the slowly varying amplitude approximation, the propagation equations of the probe and FWM fields are [48]

$$\frac{\partial \Omega_p}{\partial z} + \frac{\partial \Omega_p}{c \partial t} = \frac{ic}{2\omega_p}\nabla_\perp^2 \Omega_p + i\zeta_p(gA_3 + A_4)A_1^*, \tag{7}$$

$$\frac{\partial \Omega_m}{\partial z} + \frac{\partial \Omega_m}{c \partial t} = \frac{ic}{2\omega_m}\nabla_\perp^2 \Omega_m + i\zeta_m A_5 A_1^*, \tag{8}$$

where $\zeta_p = 2\pi N\omega_p|\mu_{31}|^2/\hbar c$ and $\zeta_m = 2\pi N\omega_m|\mu_{51}|^2/\hbar c$ are constants with N being the electron density. The first terms on the right-hand sides of the Eqs. (7) and (8) account for light diffraction. Light diffraction can be neglected if the propagation distance is much smaller than the Rayleigh range of the probe pulse or the generated FWM field, i.e. $\pi\omega_{sp(m)}^2/\lambda_{p(m)} \gg L$ [49]. In this work, we consider the propagation distance $L = 100\,\mu m$, the waist $\omega_{sp}(\omega_m) \approx 600\,\mu m$ ($200\,\mu m$) and the wavelength $\lambda_{p(m)} \approx 11.9\,\mu m$ ($4.8\,\mu m$), obtaining $\pi\omega_{sp(m)}^2/\lambda_{p(m)} \approx 9.5 \times 10^4\,\mu m$ ($2.6 \times 10^4\,\mu m$) $\gg L$. In viewing these parameters, it is safe to ignore diffraction in the following analysis.

In weak-probe regime, most of the electrons remain in the subband $|1\rangle$, i.e. $|A_1|^2 \approx 1$. Under this condition, we solve Eqs. (3)–(8) using the Fourier transform method

$$b_2\tilde{A}_2 + f\Omega_c^*\tilde{A}_3 + \Omega_c^*\tilde{A}_4 + \Omega_v^*\tilde{A}_5 = 0, \tag{9}$$

$$b_3\tilde{A}_3 + f\Omega_c\tilde{A}_2 + g\tilde{\Omega}_p = 0, \tag{10}$$

$$b_4\tilde{A}_4 + \Omega_c\tilde{A}_2 + \tilde{\Omega}_p = 0, \tag{11}$$

$$b_5\tilde{A}_5 + \Omega_v\tilde{A}_2 + \tilde{\Omega}_m = 0, \tag{12}$$

$$i\partial\tilde{\Omega}_p/\partial z - \omega\tilde{\Omega}_p/c - \zeta_p(g\tilde{A}_3 + \tilde{A}_4) = 0, \tag{13}$$

$$i\partial\tilde{\Omega}_m/\partial z - \omega\tilde{\Omega}_m/c - i\zeta_m\tilde{A}_5 = 0, \tag{14}$$

where $b_2 = \omega - \Delta_p + \Delta_c + i\gamma_2$, $b_3 = \omega - \Delta_p + \Delta + i\gamma_3$, $b_4 = \omega - \Delta_p - \Delta + i\gamma_4$ and $b_5 = \omega - \Delta_v - \Delta_p + \Delta_c + i\gamma_5$. ω is the Fourier variable. $\tilde{A}_j$ ($j = 2, 3, 4, 5$) and $\tilde{\Omega}_{p(m)}$ are the Fourier transforms of A_j ($j = 2, 3, 4, 5$) and $\Omega_{p(m)}$, respectively.

By solving Eqs. (9)–(12), one immediately obtains

$$g\tilde{A}_3 + \tilde{A}_4 = D_{p1}\tilde{\Omega}_p/D + D_{m1}\tilde{\Omega}_m/D, \tag{15}$$

$$\tilde{A}_5 = D_{p2}\tilde{\Omega}_p/D + D_{m2}\tilde{\Omega}_m/D, \tag{16}$$

where $D_{p1} = (b_3 + g^2b_4)(b_2b_5 - \Omega_v^2) - b_5(f-g)^2\Omega_c^2$, $D_{m1} = b_3\Omega_c\Omega_v^* + gfb_4\Omega_c\Omega_v^*$, $D_{p2} = b_3\Omega_c^*\Omega_v + gfb_4\Omega_c^*\Omega_v$, $D_{m2} = b_2b_3b_4 - b_3\Omega_c^2 - b_4f^2\Omega_c^2$, and $D = b_3b_4\Omega_v^2 + b_3b_5\Omega_c^2 + f^2b_4b_5\Omega_c^2 - b_2b_3b_4b_5$. By substituting Eqs. (15) and (16) into Eqs. (13) and (14) and using the initial condition $\tilde{\Omega}_m(z = 0, \omega; x, y) = 0$, we obtain the approximate solution of the FWM field

$$\tilde{\Omega}_m(z, \omega; x, y) = F\tilde{\Omega}_p(z = 0, \omega; x, y)(e^{izK_+} - e^{izK_-}), \tag{17}$$

where $K_\pm = \omega/c + (D_{m2}\zeta_m + D_{p1}\zeta_p \mp \sqrt{G})/2D = K_\pm(0) + \omega/v_{g\pm} + O(\omega^2)$, $F = \zeta_m D_{p2}/\sqrt{G}$, with $G = (D_{m2}\zeta_m - D_{p1}\zeta_p)^2 + 4D_{m1}D_{p2}\zeta_m\zeta_p$. $v_{g\pm} = 1/\text{Re}\{[\partial K_\pm(\omega)]|_{\omega=0}\}$ is the group velocity of $K_\pm$

mode. From Eq. (17), we readily see that there exist two modes described by the dispersion relations K_+ and K_-, respectively. Normally, real part $\text{Re}(K_\pm)$ is defined as the phase shifts per unit length, which reflects the variation of the phase; while imaginary part $\text{Im}(K_\pm)$ represents the absorption, which reflects the variation of the intensity [50,51].

Utilizing the inverse Fourier transform and we obtain

$$\Omega_m(z, t; x, y) = F[\Omega_p(\eta_+)e^{izK_+} - \Omega_p(\eta_-)e^{izK_-}],$$ (18)

where $\eta_\pm = t - z/v_{g_\pm}$. In the adiabatic regime, one can find the K_- mode is absorbed quickly and only the K_+ mode remains after a short propagation distance at the central frequency [52,53]. By neglecting the K_- mode, the final result of the FWM field after a short propagation distance L is obtained as

$$\Omega_m(L, t; x, y) = F\Omega_p(\eta_+)e^{iLK_+}.$$ (19)

Based on [54], the conversion efficiency of the generated FWM field can be obtained, i.e. $\eta = |E_m(L, t; x, y)/E_p(0, t; x, y)|^2$, where $E_m(L, t; x, y)$ is the electric field of the generated FWM at $z = L$ and $E_p(0, t; x, y)$ is the electric field of the probe field at $z = 0$. $|E_m(L, t; x, y)|^2 = 4\hbar^2|\Omega_m(L, t; x, y)|^2/|\mu_{51}|^2$ and $|E_p(0, t; x, y)|^2 = 4\hbar^2|\Omega_p(0, t; x, y)|^2/|\mu_{31}|^2$. Then the FWM efficiency can be written as

$$\eta = \frac{|\mu_{31}|^2}{|\mu_{51}|^2} \frac{\int_x \int_y \int_z \int_t |\Omega_m(L, t; x, y)|^2 dxdydzdt}{\int_x \int_y \int_t |\Omega_p(0, t; x, y)|^2 dxdydt}.$$ (20)

3. Results and discussion

In the following, we focus on the situation where the pump field is a LG mode $\text{LG}_{p=1}^{l=3}$. The electric density of the high-quality SQW keeps below 10^{24} m^{-3} under the case of temperatures up to 10 K [55]. In that case, we can choose the decay parameters as $\gamma_2 = 2 \times 10^{-5}$ meV, $\gamma_3 = \gamma_4 = 9$ meV and $\gamma_5 = 4$ meV.

In Fig. 2, we show the phase and intensity patterns of the FWM field when probe-field detuning Δ_p is equal to control-field detuning Δ_c. Here, Figs. 2(a) and 2(b) are phase patterns of the FWM field, while Figs. 2(c) and 2(d) are corresponding intensity patterns. As illustrated in Figs. 2(a) and 2(c), under the resonance condition $\Delta_p = \Delta_c = 0$, the phase is normal and the intensity distribution shows a double-ring pattern. Interestingly, when $\Delta_p = \Delta_c = 6$ meV, the phase remains normal and the intensity in Fig. 2(d) is the same as in Fig. 2(c). Clearly, when the condition $\Delta_p = \Delta_c$ is satisfied, the absorption is suppressed and the phase variations induced by Δ_p and Δ_c are nearly balanced out. In order to gain deeper insight into the above phenomena, we plot the real and imaginary parts of the dispersion relation K_+ as a function of radial radius r in Figs. 2(e) and 2(f). One can see the values of real parts (solid lines) are very small while the imaginary parts (dotted lines) are same in Figs. 2(e) and 2(f). Therefore, the helical phase is normal while the intensity is unchanged.

For exploring the vortex FWM process, we study the phase and intensity patterns of the FWM field when probe-field detuning Δ_p is not equal to control-field detuning Δ_c. As shown in Figs. 3(a)–3(d), when $(\Delta_p, \Delta_c) = (4, 0$ meV) or $(\Delta_p, \Delta_c) = (0, 4$ meV), the phase becomes twisted and the intensity decreases obviously compared with the Figs. 2(a)–2(d). The reason is due to the probe-field detuning Δ_p and control-field detuning Δ_c modify the spatial-dependent absorption and phase properties of the FWM field. Similarly, we give the real and imaginary parts of the dispersion relation K_+ as a function of radial radius r in Figs. 3(e) and 3(f). One can find that the real and imaginary parts increase significantly, which means that the spatial dependency of helical phase on xy space becomes stronger and the absorption is increasing. So the phase appears twisted and the intensity decreases in Figs. 3(a)–3(d). Here, note that the value of real

part in Fig. 3(e) is negative compared to the positive value of real part in Fig. 3(f), which gives the physical reason that the twisted directions of the phase patterns are opposite in Figs. 3(a) and 3(b).

In order to clearly understand the vortex mechanism, we perform the interference between the FWM field and a same-frequency Gaussian beam $\Omega_G = \Omega_{G0} \exp(-r^2/4\omega_0^2)$ for different probe-field detuning Δ_p and control-field detuning Δ_c in Fig. 4. From this figure, it can be seen that the interference phase and intensity patterns are quite different from the cases in Figs. 2 and 3. Specially, as shown in Figs. 4(g) and 4(h), the interference intensity patterns are twisted and rotated oppositely. The reason is that, due to the equiphase surface of Gaussian beam is a plane, the detunings Δ_p and Δ_c modify the phase difference between the vortex FWM field and Gaussian beam, which results in the twisted and rotated interference patterns. Actually, the results imply that one can indeed manipulate the vortex phase and intensity of the output FWM field via the probe-field detuning Δ_p or the control-field detuning Δ_c.

Finally, we study the FWM conversion efficiency η as a function of the propagation distance L, control field Ω_c, and probe-field detuning Δ_p in Figs. 5(a), 5(b) and 5(c), respectively. As shown in Fig. 5(a), it is found that the maximum FWM conversion efficiency achieves
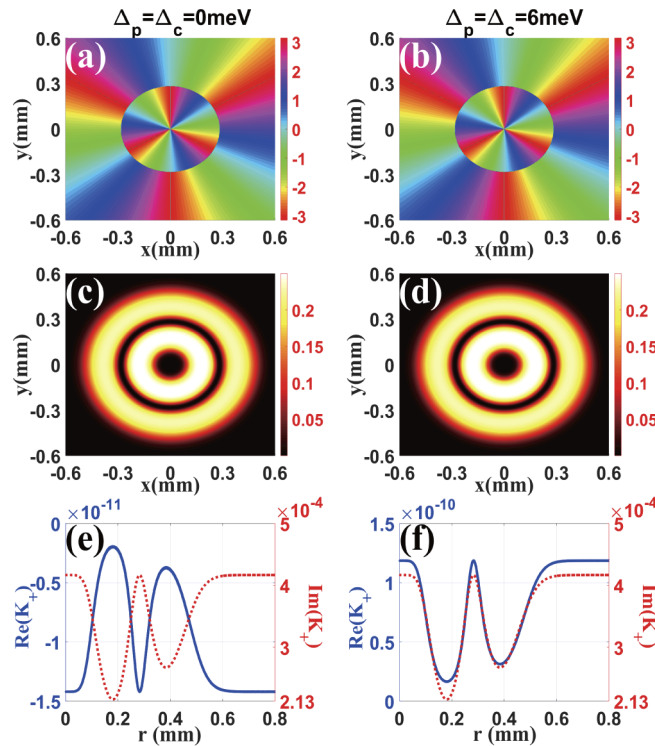
Fig. 2. Phase [(a) and (b)] and intensity [(c) and (d)] patterns of the FWM field for $\Delta_p = \Delta_c = 0$ meV and $\Delta_p = \Delta_c = 6$ meV, respectively. (e) and (f) are corresponding real Re(K_+) and imaginary Im(K_+) parts of the dispersion relation K_+ as a function of radial radius r. The other parameters are $g = f = 1.2$, $\Delta_v = 0$, $\Delta = 3$ meV, $\Omega_c = 12$ meV, $\Omega_{v0} = 15$ meV, $\zeta_m = \zeta_p = 3$ meV/μm, $\Omega_0 = 1$ meV, $l = 3$, $p = 1$, $\omega_0 = 200$ μm, $\omega_{sp} = 3\omega_0$, $\tau = 10^{-6}$ s, $L = 100$ μm.
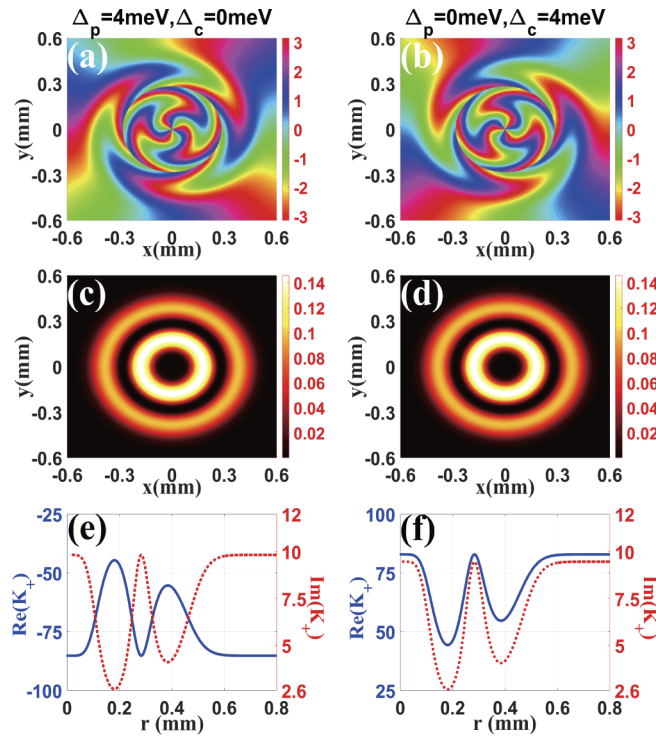
Fig. 3. Phase [(a) and (b)] and intensity [(c) and (d)] patterns of the FWM field for $(\Delta_p, \Delta_c) = (4, 0 \text{ meV})$ and $(\Delta_p, \Delta_c) = (0, 4 \text{ meV})$, respectively. (e) and (f) are corresponding real $\text{Re}(K_+)$ and imaginary $\text{Im}(K_+)$ parts of the dispersion relation K_+ as a function of radial radius r. Other parameters are the same as in Fig. 2.

approximately 36% when Δ_p is equal to Δ_c. However, when $\Delta_p \neq \Delta_c$, the maximum FWM conversion efficiency decreases dramatically with the increasing propagation distance L. In the Fig. 5(b), we display the FWM conversion efficiency η as a function of the control field Ω_c for different Δ_p and Δ_c. Interestingly, when $\Delta_p = \Delta_c$, the maximum FWM conversion efficiency achieves nearly 50%. On the contrary, for the case $\Delta_p \neq \Delta_c$, the maximum FWM conversion efficiency decreases by approximately 30%. Also, we plot the FWM conversion efficiency η vs probe-field detuning Δ_p in Fig. 5(c). From this figure, one can see the FWM conversion efficiency keeps fixed (solid line) when $\Delta_p = \Delta_c$ and reaches the maximum value at the point $\Delta_p = 4$ meV (dotted line) in the case $\Delta_p \neq \Delta_c$. The above results demonstrate, when the condition $\Delta_p = \Delta_c$ is satisfied, the absorption is significantly suppressed and the phase variations induced by Δ_p and Δ_c are balanced out, then the high FWM conversion efficiency is achieved even the propagation distance is very long, i.e. $L = 400 \, \mu$m. Therefore, our study may open up a new way for realizing the high-efficiency long-distance multi-channel information transfer [56] in a solid.
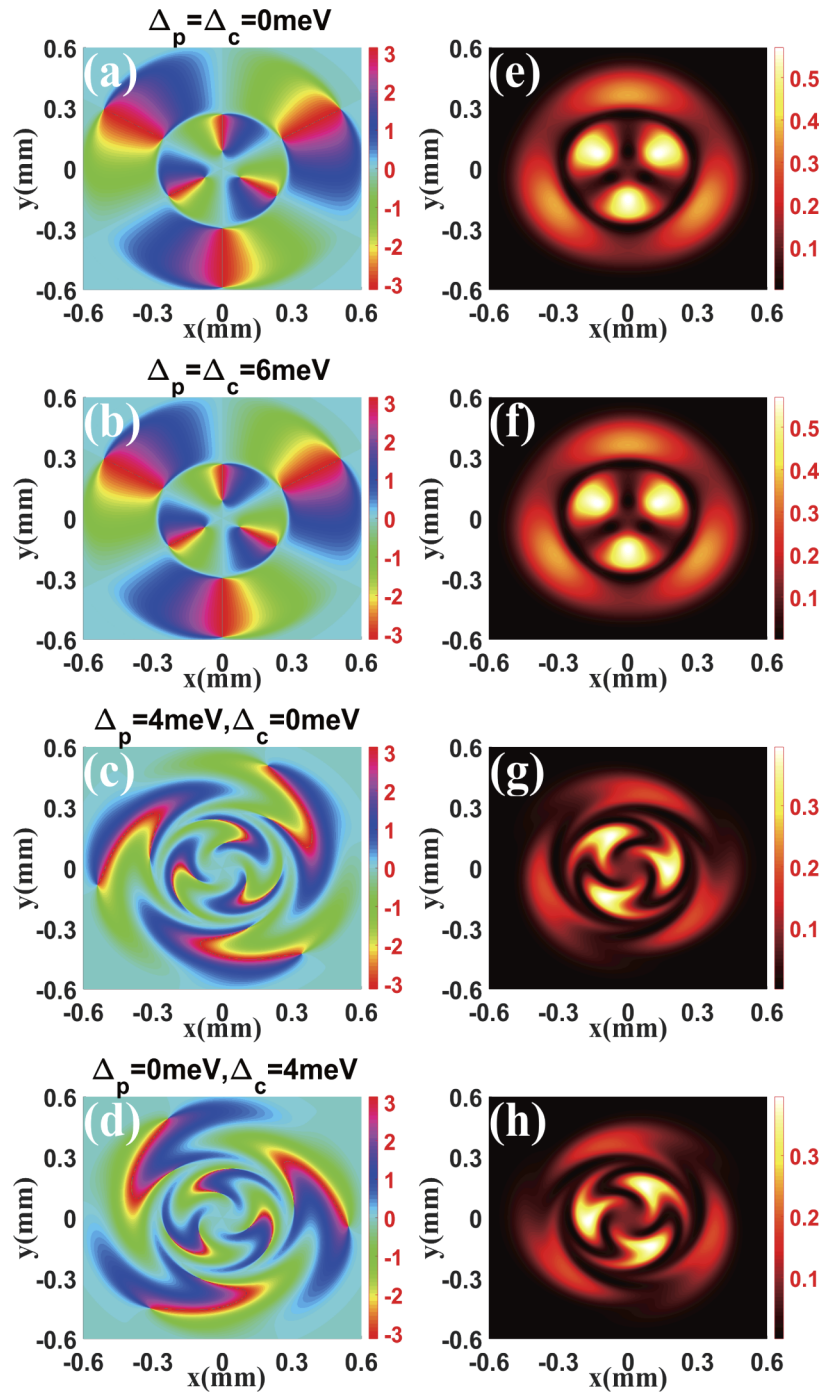
Fig. 4. Interference phase (a)–(d) and intensity (e)–(h) patterns of the FWM field and a same-frequency Gaussian beam for different probe-field detuning Δ_p and the control-field detuning Δ_c. Other parameters are the same as in Fig. 2 except for $\Omega_{G0} = 0.3$ meV. Note that, profiles (a)–(d) have shown the evidence that OAM phase is transferred entirely from the pump field to the FWM field, while profiles (a)–(h) imply that both the intensity and the phase of the FWM field are modulated.
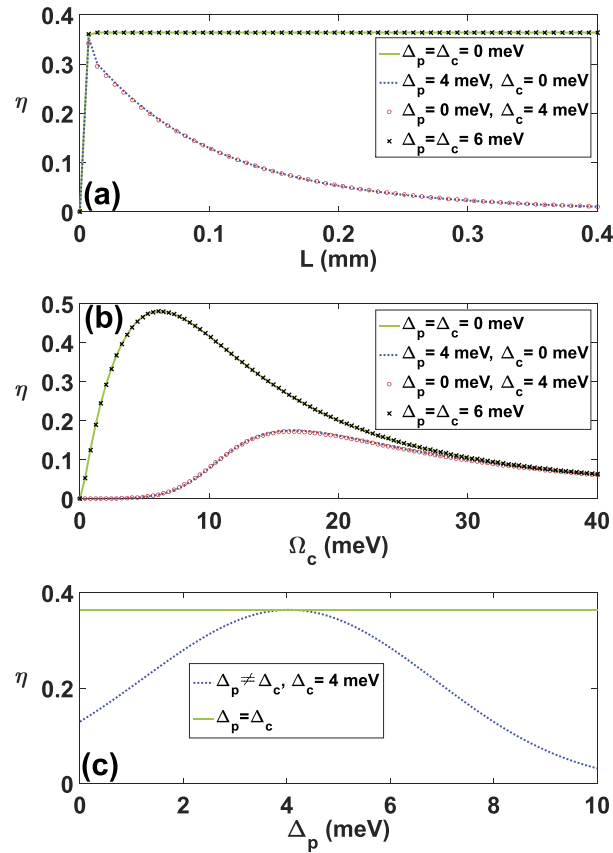
Fig. 5. The FWM conversion efficiency η as a function of the propagation distance L (a), control field Ω_c (b), and probe-field detuning Δ_p (c), respectively. Other parameters are the same as in Fig. 2.

4. Conclusion

In the present study, we mainly focus on the condition of low temperatures up to 10 K, and have neglected other many-body effects such as the depolarization effect, which renormalizes the free-carrier and carrier-field contributions. These contributions and their interplay have been investigated quite thoroughly in [57]. Note that, due to the small carrier density considered here, these effects only give a negligible correction.

In conclusion, we have demonstrated a new scheme to achieve highly efficient vortex FWM in asymmetric semiconductor quantum wells where strong cross coupling between neighboring wells are considered. Owing to the inter-well cross coupling, one can effectively manipulate the helical phase and intensity of the FWM field via the probe-field detuning and control-field detuning. More importantly, when probe-field detuning is equal to control-field detuning, the highly efficient vortex FWM is achieved and the maximum FWM conversion efficiency is approximately 50%. As a result, the method and theoretical analyses that are proposed here may open novel avenues to investigate OAM-based phenomena in different nanostructures [58–64] .

Disclosures

The authors declare that they have no conflict of interest.

References

1. L. Allen, M. W. Beijersbergen, R. J. C. Spreeuw, and J. P. Woerdman, "Orbital angular momentum of light and the transformation of Laguerre-Gaussian laser modes," Phys. Rev. A **45**(11), 8185–8189 (1992).
2. M. Padgett, J. Courtial, and L. Allen, "Light's orbital angular momentum," Phys. Today **57**(5), 35–40 (2004).
3. A. Mair, A. Vaziri, G. Weihs, and A. Zeilinger, "Entanglement of the Orbital Angular Momentum States of Photons," Nature (London) **412**(6844), 313–316 (2001).
4. D. G. Grier, "A revolution in optical manipulation," Nature **424**(6950), 810–816 (2003).
5. G. Molina-Terriza, J. P. Torres, and L. Torner, "Twisted photons," Nat. Phys. **3**(5), 305–310 (2007).
6. M. Padgett and R. Bowman, "Tweezers with a twist," Nat. Photonics **5**(6), 343–348 (2011).
7. J. Wang, J. Y. Yang, I. M. Fazal, N. Ahmed, Y. Yan, H. Huang, Y. Ren, Y. Yue, S. Dolinar, and M. Tur, "Terabit free-space data transmission employing orbital angular momentum multiplexing," Nat. Photonics **6**(7), 488–496 (2012).
8. D. S. Ding, Z. Y. Zhou, B. S. Shi, and G. C. Guo, "Single-photon-level quantum image memory based on cold atomic ensembles," Nat. Commun. **4**(1), 2527 (2013).
9. A. Nicolas, L. Veissier, L. Giner, E. Giacobino, D. Maxein, and J. Laurat, "A quantum memory for orbital angular momentum photonic qubits," Nat. Photonics **8**(3), 234–238 (2014).
10. V. Parigi, V. Ambrosio, C. Arnold, L. Marrucci, F. Sciarrino, and J. Laurat, "Storage and retrieval of vector beams of light in a multiple-degree-of-freedom quantum memory," Nat. Commun. **6**(1), 7706 (2015).
11. A. M. Marino, V. Boyer, R. C. Pooser, P. D. Lett, K. Lemons, and K. M. Jones, "Delocalized Correlations in Twin Light Beams with Orbital Angular Momentum," Phys. Rev. Lett. **101**(9), 093602 (2008).
12. J. Ruseckas, V. Kudriasov, I. A. Yu, and G. Juzeliunas, "Transfer of orbital angular momentum of light using two-component slow light," Phys. Rev. A **87**(5), 053840 (2013).
13. N. Radwell, T. W. Clark, B. Piccirillo, S. M. Barnett, and S. Franke-Arnold, "Spatially Dependent Electromagnetically Induced Transparency," Phys. Rev. Lett. **114**(12), 123603 (2015).
14. G. Walker, A. S. Arnold, and S. Franke-Arnold, "Trans-Spectral Orbital Angular Momentum Transfer via Four-Wave Mixing in Rb Vapor," Phys. Rev. Lett. **108**(24), 243601 (2012).
15. D. Zhang, X. Liu, L. Yang, X. Li, Z. Zhang, and Y. Zhang, "Modulated vortex six-wave mixing," Opt. Lett. **42**(16), 3097–3100 (2017).
16. A. Imamoğlu and R. J. Ram, "Semiconductor lasers without population inversion," Opt. Lett. **19**(21), 1744–1746 (1994).
17. D. E. Nikonov, A. Imamoğlu, and M. O. Scully, "Fano interference of collective excitations in semiconductor quantum wells and lasing without inversion," Phys. Rev. B **59**(19), 12212–12215 (1999).
18. M. D. Frogley, J. F. Dynes, M. Beck, J. Faist, and C. C. Phillips, "Gain without inversion in semiconductor nanostructures," Nat. Mater. **5**(3), 175–178 (2006).
19. S. M. Sadeghi, H. M. van Driel, and J. M. Fraser, "Coherent control and enhancement of refractive index in an asymmetric double quantum well," Phys. Rev. B **62**(23), 15386–15389 (2000).
20. J. F. Dynes, M. D. Frogley, J. Rodger, and C. C. Phillips, "Optically mediated coherent population trapping in asymmetric semiconductor quantum wells," Phys. Rev. B **72**(8), 085323 (2005).
21. M. C. Phillips and H. Wang, "Spin Coherence and Electromagnetically Induced Transparency via Exciton Correlations," Phys. Rev. Lett. **89**(18), 186401 (2002).
22. M. C. Phillips and H. Wang, "Electromagnetically induced transparency due to intervalence band coherence in a GaAs quantum well," Opt. Lett. **28**(10), 831–833 (2003).
23. P.-C. Ku, F. Sedgwick, C. J. Chang-Hasnain, P. Palinginis, T. Li, H. Wang, S.-W. Chang, and S.-L. Chuang, "Slow light in semiconductor quantum wells," Opt. Lett. **29**(19), 2291–2293 (2004).
24. H. Sun, S. Gong, Y. Niu, S. Jin, R. Li, and Z. Xu, "Enhancing Kerr nonlinearity in an asymmetric double quantum well via Fano interference," Phys. Rev. B **74**(15), 155314 (2006).

25. H. Sun, Y. Niu, R. Li, S. Jin, and S. Gong, "Tunneling-induced large cross-phase modulation in an asymmetric quantum well," Opt. Lett. **32**(17), 2475–2477 (2007).

26. J. H. Li, "Controllable optical bistability in a four-subband semiconductor quantum well system," Phys. Rev. B **75**(15), 155329 (2007).

27. W. X. Yang, J. M. Hou, and R. K. Lee, "Ultraslow bright and dark solitons in semiconductor quantum wells," Phys. Rev. A **77**(3), 033838 (2008).

28. C. J. Zhu and G. X. Huang, "Slow-light solitons in coupled asymmetric quantum wells via interband transitions," Phys. Rev. B **80**(23), 235408 (2009).

29. X. Hao, J. Li, J. Liu, P. Song, and X. Yang, "Efficient four-wave mixing of a coupled double quantum-well nanostructure," Phys. Lett. A **372**(14), 2509–2513 (2008).

30. S. Evangelou and E. Paspalakis, "Pulsed four-wave mixing in intersubband transitions of a symmetric semiconductor quantum well," Photonics Nanostruct.: Fundam. Appl. **9**(2), 168–173 (2011).

31. S. G. Kosionis, A. F. Terzis, and E. Paspalakis, "Transient four-wave mixing in intersubband transitions of semiconductor quantum wells," J. Lumin. **140**, 130–134 (2013).

32. S. Liu, W. X. Yang, Y. L. Chuang, A. X. Chen, A. Liu, and Y. Huang, "Enhanced four-wave mixing efficiency in four-subband semiconductor quantum wells via Fano-type interference," Opt. Express **22**(23), 29179–29190 (2014).

33. S. E. Harris and L. V. Hau, "Nonlinear Optics at Low Light Levels," Phys. Rev. Lett. **82**(23), 4611–4614 (1999).

34. L. Deng, M. Kozuma, E. W. Hagley, and M. G. Payne, "Opening Optical Four-Wave Mixing Channels with Giant Enhancement Using Ultraslow Pump Waves," Phys. Rev. Lett. **88**(14), 143902 (2002).

35. Y. Zhang, A. W. Brown, and M. Xiao, "Opening Four-Wave Mixing and Six-Wave Mixing Channels via Dual Electromagnetically Induced Transparency Windows," Phys. Rev. Lett. **99**(12), 123603 (2007).

36. Z. Qin, L. Cao, H. Wang, A. M. Marino, W. Zhang, and J. Jing, "Experimental Generation of Multiple Quantum Correlated Beams from Hot Rubidium Vapor," Phys. Rev. Lett. **113**(2), 023602 (2014).

37. Y. Hong, Z. Wang, D. Ding, and B. Yu, "Ultraslow vortex four-wave mixing via multiphoton quantum interference," Opt. Express **27**(21), 29863–29874 (2019).

38. X. Pan, S. Yu, Y. Zhou, K. Zhang, K. Zhang, S. Lv, S. Li, W. Wang, and J. Jing, "Orbital-Angular-Momentum Multiplexed Continuous-Variable Entanglement from Four-Wave Mixing in Hot Atomic Vapor," Phys. Rev. Lett. **123**(7), 070506 (2019).

39. J. Faist, F. Capassom, C. Sirtori, K. W. West, and L. N. Pfeiffer, "Controlling the sign of quantum interference by tunnelling from quantum wells," Nature **390**(6660), 589–591 (1997).

40. J. H. Wu, J. Y. Gao, J. H. Xu, L. Silvestri, M. Artoni, G. C. La Rocca, and F. Bassani, "Ultrafast All Optical Switching via Tunable Fano Interference," Phys. Rev. Lett. **95**(5), 057401 (2005).

41. H. Sun, S. Fan, H. Zhang, and S. Gong, "Tunneling-induced high-efficiency four-wave mixing in asymmetric quantum wells," Phys. Rev. B **87**(23), 235310 (2013).

42. A. M. Yao and M. J. Padgett, "Orbital angular momentum: origins, behavior and applications," Adv. Opt. Photonics **3**(2), 161–204 (2011).

43. D. E. Nikonov, A. Imamoğlu, L. V. Butov, and H. Schmidt, "Collective Intersubband Excitations in Quantum Wells: Coulomb Interaction versus Subband Dispersion," Phys. Rev. Lett. **79**(23), 4633–4636 (1997).

44. M. O. Scully and M. S. Zubairy, *Quantum Optics* (Cambridge University, Cambridge, UK, 1997).

45. G. B. Serapiglia, E. Paspalakis, C. Sirtori, K. L. Vodopyanov, and C. C. Phillips, "Laser-Induced Quantum Coherence in a Semiconductor Quantum Well," Phys. Rev. Lett. **84**(5), 1019–1022 (2000).

46. M. C. Phillips, H. Wang, I. Rumyantsev, N. H. Kwong, R. Takayama, and R. Binder, "Electromagnetically Induced Transparency in Semiconductors via Biexciton Coherence," Phys. Rev. Lett. **91**(18), 183602 (2003).

47. E. Paspalakis, M. Tsaousidou, and A. F. Terzis, "Coherent manipulation of a strongly driven semiconductor quantum well," Phys. Rev. B **73**(12), 125344 (2006).

48. T. N. Dey and J. Evers, "Nondiffracting optical beams in a three-level Raman system," Phys. Rev. A **84**(4), 043842 (2011).

49. Y. Zhang, Z. Wang, J. Qiu, Y. Hong, and B. Yu, "Spatially dependent four-wave mixing in semiconductor quantum wells," Appl. Phys. Lett. **115**(17), 171905 (2019).

50. Y. Wu, J. Saldana, and Y. Zhu, "Large enhancement of four-wave mixing by suppression of photon absorption from electromagnetically induced transparency," Phys. Rev. A **67**(1), 013811 (2003).

51. L.-G. Si, W.-X. Yang, X. Y. Lü, X. Hao, and X. Yang, "Formation and propagation of ultraslow three-wave-vector optical solitons in a cold seven-level triple-Λ atomic system under Raman excitation," Phys. Rev. A **82**(1), 013836 (2010).

52. Y. Wu, M. G. Payne, E. W. Hagley, and L. Deng, "Efficient multiwave mixing in the ultraslow propagation regime and the role of multiphoton quantum destructive interference," Opt. Lett. **29**(19), 2294–2296 (2004).

53. H. Li and G. Huang, "Highly efficient four-wave mixing in a coherent six-level system in ultraslow propagation regime," Phys. Rev. A **76**(4), 043809 (2007).

54. Y. Wu and X. Yang, "Highly efficient four-wave mixing in double-Λ system in ultraslow propagation regime," Phys. Rev. A **70**(5), 053818 (2004).

55. H. C. Liu and F. Capasso, *Intersubband Transitions in Quantum Wells: Physics and Device Applications* (Academic, New York, 2000).

56. G. Gibson, J. Courtial, M. J. Padgett, M. Vasnetsov, V. Pas'ko, S. M. Barnett, and S. Franke-Arnold, "Free-space information transfer using light beams carrying orbital angular momentum," Opt. Express **12**(22), 5448–5456 (2004).

57. T. Shih, K. Reimann, M. Woerner, T. Elsaesser, I. Waldmüller, A. Knorr, R. Hey, and K. H. Ploog, "Nonlinear response of radiatively coupled intersubband transitions of quasi-two-dimensional electrons," Phys. Rev. B **72**(19), 195338 (2005).

58. S. M. Sadeghi, L. Deng, X. Li, and W. P. Huang, "Plasmonic (thermal) electromagnetically induced transparency in metallic nanoparticle-quantum dot hybrid systems," Nanotechnology **20**(36), 365401 (2009).

59. S. M. Sadeghi, "Gain without inversion in hybrid quantum dot-metallic nanoparticle systems," Nanotechnology **21**(45), 455401 (2010).

60. M. R. Singh, D. G. Schindel, and A. Hatef, "Dipole-dipole interaction in a quantum dot and metallic nanorod hybrid system," Appl. Phys. Lett. **99**(18), 181106 (2011).

61. H. S. Borges, L. Sanz, J. M. Villas-Bôas, O. O. Diniz Neto, and A. M. Alcalde, "Tunneling induced transparency and slow light in quantum dot molecules," Phys. Rev. B **85**(11), 115425 (2012).

62. S. M. Sadeghi, W. J. Wing, and R. R. Gutha, "Undamped ultrafast pulsation of plasmonic fields via coherent exciton-plasmon coupling," Nanotechnology **26**(8), 085202 (2015).

63. F. Carreño, M. A. Antón, V. Yannopapas, and E. Paspalakis, "Control of the absorption of a four-level quantum system near a plasmonic nanostructure," Phys. Rev. B **95**(19), 195410 (2017).

64. I. Thanopulos, V. Karanikolas, N. Iliopoulos, and E. Paspalakis, "Non-Markovian spontaneous emission dynamics of a quantum emitter near a MoS$_2$ nanodisk," Phys. Rev. B **99**(19), 195412 (2019).